

# The relation between QSO absorption systems and high redshift galaxies

Matthias Steinmetz

<sup>1</sup>*Steward Observatory, University of Arizona, Tucson, AZ 85721, USA*

**Abstract.** The relation between high redshift galaxies and QSO absorption systems is discussed in the context of hierarchical galaxy formation. It is demonstrated that imprints of the reionization history of the universe are detectable in the  $b$ -parameter distribution of the Ly- $\alpha$  forest at redshifts two to four, favoring models in which hydrogen and helium are reionized simultaneously at or before redshift five by a quasar-like spectrum of UV photons. Hydrodynamical simulations including star formation, feedback due to supernovae and chemical enrichment are also presented. Energy feedback in form of kinetic energy can give rise to an efficient transport of metals out to distances of a few hundred kpc. The observational signature of this metal transport mechanism compared to simple homogeneous enrichment models is discussed. Finally, it is shown that present day  $L^*$  galaxies typically have several progenitors at  $z \approx 3$  spread over a few hundred kpc. These progenitors are closely associated with damped Ly- $\alpha$  and Ly-limit systems, and have velocity dispersions, luminosities and colors comparable to U-dropout galaxies at  $z \approx 3$ .

## 1 Introduction

Over the past few years gasdynamical simulations have had an enormous impact on our theoretical understanding of QSO absorption systems. These simulations can explain the basic properties of QSO absorbers covering many orders of magnitude in column density (see, e.g., the many simulation related contributions in this volume). While the lowest column density systems ( $\log N_{\text{HI}} \approx 12-14$ ) arises from gas in voids and sheets of the “cosmic web”, systems of higher column density are produced by filaments ( $\log N \approx 14-17$ ) or even gas which has cooled and collapsed in virialized halos ( $\log N > 17$ ). So far, numerical simulations have been applied primarily to systems with lower column densities ( $\log N \lesssim 17$ ), corresponding to gas densities below  $10^{-2} \text{ cm}^{-3}$ . At these low densities the important physical processes are relatively simple and well understood. Fluctuations are still only mildly non-linear and the gas is essentially in photoionization equilibrium with the UV background. Cooling times are long compared to dynamical time scales.

These simulations have so far neglected the effects of star formation and related feedback processes. They thus suffer from the overcooling problem, which results in disk galaxies which are too massive/luminous and too concentrated compared with present day spiral galaxies [1]. This problem may be overcome by including an efficient heating mechanism as, e.g., energy feedback

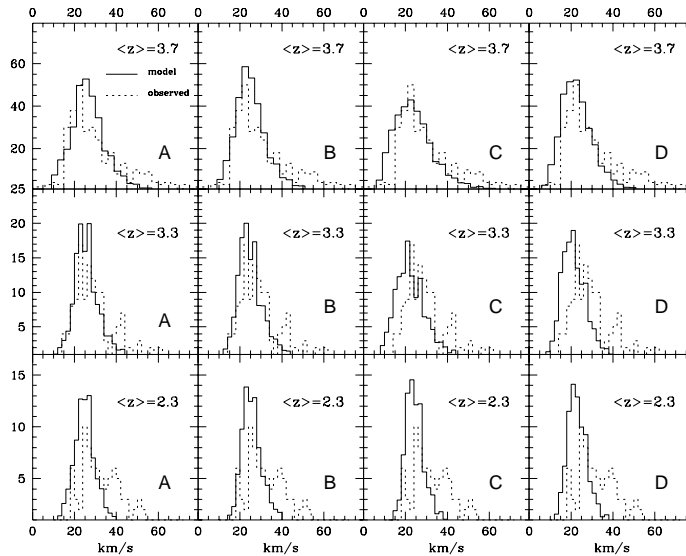


Figure 1: Observed (dashed line) and simulated (solid line) Doppler parameter distributions for models A–D (from left to right). The mean redshift of the samples is  $\langle z \rangle = 2.3, 3.3, 3.7$ .

from supernovae. Metals ejected from star-forming galaxies in the process of formation also provide an attractive scenario to explain the pollution of the IGM with metals. However, shocks caused by this outflowing gas may also dramatically affect the thermodynamics of the intergalactic medium.

In this contribution, I will present some examples how non-equilibrium thermodynamics and star formation may affect properties of QSO absorption systems. In a first application (section 2) the influence of the reionization history of the universe on the thermodynamics of the IGM is discussed. Section 3 shows to what extent winds driven by energy feedback due to supernovae can pollute the intergalactic medium with metals. Section 4 addresses the relation between high column density absorbers and the population of local and high redshift galaxies.

## 2 Disentangling the reionization history of the universe

This section investigates how non-equilibrium thermodynamics may affect properties of the Ly- $\alpha$  forest, in particular the  $b$ -parameter distribution and its dependence on the reionization history of the universe [2]. During reionization the IGM is heated up due to the residual energy of photons absorbed by

hydrogen and helium. Cooling due to Compton scattering (at  $z \gtrsim 5$ ) and due to adiabatic expansion continuously lowers the temperature until photoheating and cooling are in equilibrium. During the epoch between reionization and equilibrium, the temperature-density distribution of the IGM depends on the exact balance between these heating and cooling processes. Different reionization histories thus result in different  $\rho - T$  relations at low densities. These differences may be observable by comparing the simulated and observed  $N - b$  relation ( $b$ -parameter distribution). Such a comparison requires to follow self-consistently the non-equilibrium evolution of the baryonic species (H,  $H^+$ , He,  $He^+$ ,  $He^{++}$ , and  $e^-$ ). It is further complicated by the fact the  $b$  parameter is typically dominated by bulk motions rather than the IGM's temperature.

In order to demonstrate that different ionization histories can leave some observable imprints in the  $b$ -parameter distribution, four different models have been simulated to cover the uncertainty concerning the respective role of quasars and stars in the reionization of the Universe:

Model A: Ionizing background as proposed by Haardt & Madau [3]. The spectrum is a power-law with  $\alpha=1.5$  processed by the intervening Ly- $\alpha$  absorption.

Model B: Same as model A but the redshift evolution is stretched towards higher redshift.

Model C: Same as model A but the redshift evolution is compressed towards lower redshift. A stellar component is added to the UV background which reionizes hydrogen at redshift  $z \sim 6$  with a soft spectrum (power law with  $\alpha=5$ ).

Model D: Same as C but the stellar component reionizes hydrogen at redshift  $z \sim 30$ .

Model A was chosen by Haardt & Madau [3] to represent the UV background due to observed quasars. Model B mimics the existence of an as yet undetected population of quasar at redshifts beyond five. Models C and D address the possibility that the Haardt & Madau model overestimates the UV background due to quasars at redshifts larger than three. In the latter case the UV background would have to be dominated by a stellar contribution at these redshifts.

The simulations are performed using GRAPESPH [4] a smoothed particle hydrodynamics code which includes the relevant cooling and heating processes and follows self-consistently the non-equilibrium evolution of the baryonic species (H,  $H^+$ , He,  $He^+$ ,  $He^{++}$ , and  $e^-$ ). The Doppler parameters were obtained by fitting Voigt profiles to artificial spectra with the automatic line fitting program AUTOVP kindly provided by Romeel Davé [5].

Figure 1 compares observed and simulated Doppler parameter distribution at three different redshifts [6, 7]. The mean redshift and the column density

range of the sample of lines identified in the artificial spectra has been matched to those of observed samples. At high redshift ( $\langle z \rangle = 3.3, 3.7$ ) there is good agreement between the observed and simulated Doppler parameter distribution in the case of models A and B. The only discrepancy is a modest high-velocity tail which is present in the observed data but not in the simulated distribution. Models C and D clearly disagree with the observed distribution. They show a considerable fraction of lines which are cooler than the lower cut-off of 15 km/s. At redshift 2.3 there is a significant discrepancy between simulated and observed distribution for all four models. The observed distribution shows a pronounced high-velocity tail which is not reproduced by any of the models. The failure to reproduce the high-velocity tail may be related to the too small a box size of the simulation which thus miss larger-scale bulk motions [8]. An alternative interpretation is that simulations significantly underestimate the fraction of the IGM in a hot collisionally ionized phase because they do not include any feedback effects due to star formation.

### 3 Metal Enrichment of the IGM

The simulations in this and the next section include star formation and the effects of energy feedback due to supernovae. Star formation is modelled by a heuristic scheme in which high density, rapidly cooling gas is transformed into stars assuming a Miller-Scalo IMF. Stars more massive than  $8 M_{\odot}$  are assumed to explode as Type II supernovae and deposit locally  $\approx 10^{51}$  erg into the ISM. A fraction  $f_v$  (typically about 10%) of this energy is invested in modifying the kinetic energy of the surrounding gas while the remaining  $(1 - f_v)$  heats up the neighboring gas. Furthermore, supernovae also enrich neighboring fluid elements with metals. More details on the star formation algorithm are given in [9] and [10].

Figure 2 shows CIV column density maps for redshift 3 and 4 for three different enrichment scenarios. The model shown in the left panels assumes a homogeneous enrichment with a metallicity of  $[Z] = -2.5$ . The properties of metal-line systems arising in such a model have been shown to match observations fairly well [11, 12]. It also predicts at  $z = 3$  a high fraction of metal-line systems for HI column densities above  $\log N = 15$ , consistent with observations. In the simulations shown in the middle and right panel, star formation and enrichment is treated self-consistently but with different feedback parameters,  $f_v = 0$  (pure thermal feedback) for the models shown in the middle column and  $f_v = 0.1$  for the models shown in the right column. Models with  $f_v = 0.1$  have also been shown to reproduce the present day galaxy luminosity function [13]. In the thermal feedback model, the metal distribution is very concentrated towards the center of galaxies where stars are actually formed. Only a small fraction of LOS with  $\log N(HI) > 15$  would show an detectable CIV absorption, inconsistent with observations. This flaw is cured in the turbulent feedback model, which at  $z \approx 3$  shows an absorption fraction

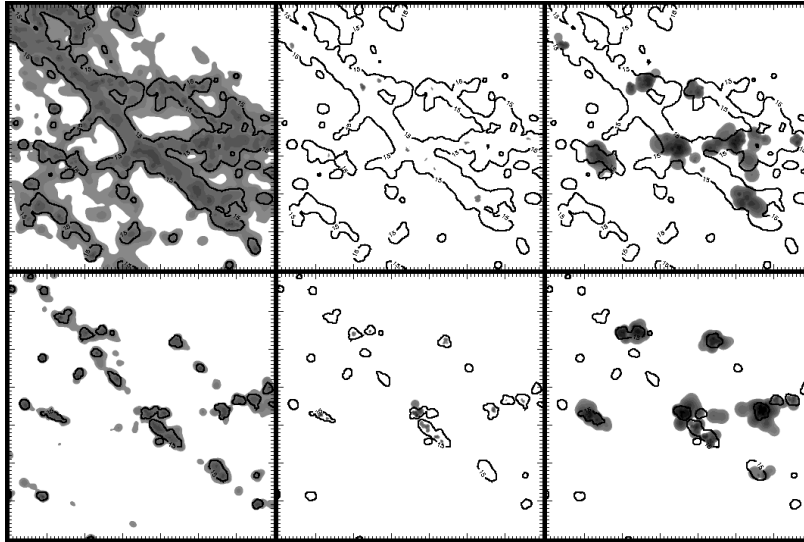


Figure 2: CIV column density distribution for  $z = 4$  (top row) and  $z = 3$  (bottom row). The left column corresponds to a model assuming a constant, homogeneously distributed metallicity ( $[Z] = -2.5$ ), the middle column to a model with feedback due to thermal energy ( $f_v = 0$ ), the right column to a model with feedback due to thermal and turbulent energy ( $f_v = 0.1$ ). The solid contour line encloses regions with a HI column density of above  $\log N = 15$ , the gray shaded region marks a CIV column density of  $\log N > 11.7$ . The size of each frame is 2.8 Mpc comoving.

similar to that of the homogeneous model, though the correlation between HI and CIV absorption is weaker. Considering the redshift evolution opens an interesting opportunity to discriminate between these different enrichment scenarios. The area enclosed by the  $\log N(HI) > 15$  contour increases substantially going from redshift 3 to 4. Similarly the area with  $\log N(CIV) > 11.7$  increases for the homogeneous enrichment model. Contrary, this area is about constant, if not decreasing with redshift for the two feedback models. Translated into the  $dN/dz$  relation for CIV, the homogeneous enrichment model predicts a strong increase with redshift while the two feedback models predict  $dN_{CIV}/dz \approx const.$

It should be noted that these results are in partial disagreement with simulation recently done by Gnedin [14], who finds a substantially weaker effect of supernovae feedback, but a stronger ejection of metals due to dynamics. While the differences in the simulation including supernovae feedback can be likely accounted to the different star formation and feedback models, the origin

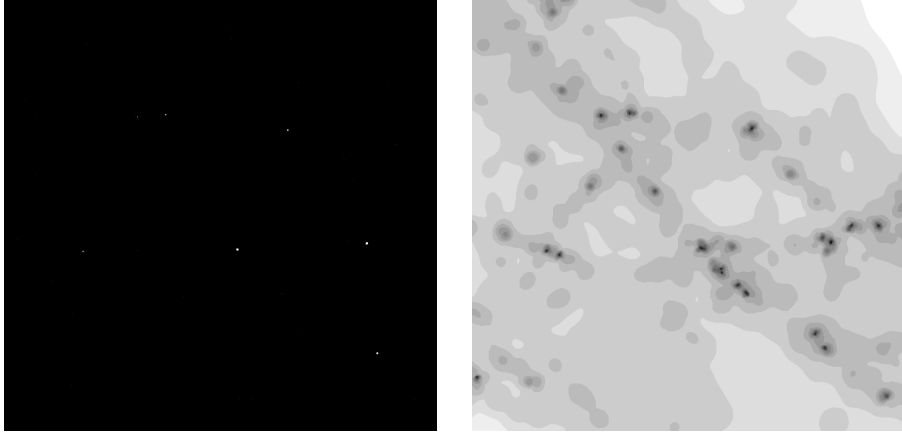


Figure 3: Left: Artificial I-band image of a galaxy in the process of formation  $z \approx 3$  in an HDF like exposure. Resolution, Noise, PSF and efficiency are taken to match that of the HST WFPC2 camera. Right: HI column density map at  $z=3$ . Each frame has a sidelength of 2.8 Mpc (comoving).

of the differences if supernovae feedback is minimized is much less clear and requires further investigation.

#### 4 The connection between present day, galaxies, high- $z$ galaxies and QSO absorption systems

The simulation presented in the last section can also be used to investigate further the relation between QSO absorbers and galaxies in the process of formation. Each “star” particle corresponds to a population of about  $10^6$  stars formed in a star-burst manner. By means of spectro-photometric models [15], predictions for the emission of these galaxies in the broad-band colors UBVRIK can be made.

In Figure 3, a HI column density map is compared with such an synthetic I-band image of the stellar component. The I band image includes noise, PSF and exposure time similar to that of the Hubble Deep Field. The artificial image shows about 8 detectable protogalactic clumps (PGCs). Each of these PGCs is situated close to a region of very high column density ( $\log N > 17$ ). However, there is still a substantial number of Ly-limit and damped Ly- $\alpha$  systems, which do not host a stellar PGC.

Due to the small physical size of the high resolution region of the simulation, all PGCs share virtually the same redshift ( $\Delta v \approx 400$  km/sec). In total a set of about 20 galaxies has been simulated with circular velocities ranging between 100 and 200 km/s (at  $z = 0$ ). Each of these galaxies gives rise to a

couple of detectable ( $I < 26$ ) progenitors at  $z \approx 2 - 3$ , a behavior which nicely accounts for the increasing evidence for redshift clustering at redshifts above 2 [16, 17].

It is also of interest to take a closer look at further properties of these PGCs. Luminosity as well as circular velocity of the most massive clump at  $z \approx 3$  is very similar to that of its present day counterpart. The mass of the most massive progenitor is, however, only about 10% of that at the present epoch. Star formation rates are fairly moderate, typically a few to several solar masses per year. These characteristics are at least qualitatively in very good agreement with properties of the recently detected population of galaxies at  $z = 3$  and give some support for the hypothesis that the U-dropout galaxies are the progenitors of the present population of massive galaxies [17].

**Acknowledgements.** This article includes work from collaborations with G. Conrardo, M. Haehnelt, J. Navarro and M. Rauch.

## References

- [1] Navarro, J.F., Steinmetz, M., 1997, ApJ , 471, 13.
- [2] Haehnelt, M., Steinmetz, M., 1997, MNRAS , in press.
- [3] Haardt, F., Madau, P., 1996, ApJ , 461, 20.
- [4] Steinmetz, M., 1996, MNRAS , 278, 1005.
- [5] Davé R., Hernquist L., Weinberg D.H., Katz N., 1997, ApJ, in press.
- [6] Lu L., Sargent W.L.W., Womble D.S., Masahide T.-H., 1996, 472, 509.
- [7] Kim T.S., Hu E.M., Cowie L.L., Songaila A., 1997, AJ, in press.
- [8] Hui, L., Rutledge, R., 1997, ApJ , submitted.
- [9] Navarro, J.F., White, S.D.M., 1993, MNRAS , 265, 271.
- [10] Steinmetz, M., Müller, E., 1994, A&A , 281, L97.
- [11] Rauch, M., Haehnelt, M.G., Steinmetz, M., 1997, ApJ 481, 601.
- [12] Hellsten, U., Davé R., Hernquist, L., Weinberg D.H., Katz N., 1997, ApJ in press.
- [13] Cole, S.M., Aragón-Salamanca, A., Frenk, C.S., Navarro, J.F., Zepf, S.E. 1994, MNRAS , 271, 781.
- [14] Gnedin, N., 1997, MNRAS , in press.
- [15] Fritze-von Alvensleben, U., 1994, in *Panchromatic View of galaxies – their Evolutionary Puzzle*, eds. Hensler, G., Theis, C., Gallagher, J., Editions Frontières, p.245.
- [16] Pascarelle, S.M., Windhorst, R.A., Keel, W.C., Odewahn, S.C., Nature , 383, 45.
- [17] Steidel, C., Adelberger, K., Dickinson, M., Giavalisco M., Pettini, M., Kellogg, M., 1997, ApJ , in press.